

Biological Effects of Different Thin Layer Hydroxyapatite Coatings on Anodized Titanium

Sung-Hwa Sohn¹, Hye-Kyoung Jun²,
Chang-Su Kim², Ki-Nam Kim¹, Yeon Mi Ryu¹,
Seung Ho Lee¹, Yu-Ri Kim¹, Sang-Hui Seo¹,
Hye Won Kim¹, Sang-Wan Shin², Jae-Jun Ryu²
& Meyoung-Kon Kim¹

¹Department of Biochemistry & Molecular Biology,

²Department of Dentistry, College of Medicine, Korea University,
Seoul 136-705, Korea

Correspondence and requests for materials should be addressed
to M-K. Kim (jerrykim@korea.ac.kr)

Accepted 3 December 2005

Abstract

Several features of the implant surface, such as roughness, topography, and composition play a relevant role in implant integration with bone. This study was conducted in order to determine the effects of various thin layer hydroxyapatite (HA) coatings on anodized Ti surfaces on the biological responses of a human osteoblast-like cell line (MG63). MG63 cells were cultured on A (100 nm HA coating on anodized surface), B (500-700 nm HA coating on anodized surface), C (1 μ m HA coating on anodized surface), and control (non HA coating on anodized surface) Ti. The morphology of these cells was assessed by SEM. The cDNAs prepared from the total RNAs of the MG63 were hybridized into a human cDNA microarray (1,152 elements). The appearances of the surfaces observed by SEM were different on each of the four dental substrate types. MG63 cells cultured on A, C and control exhibited cell-matrix interactions. It was B surface showing cell-cell interaction. In the expression of several genes were up-, and down-regulated on the different surfaces. The attachment and expression of key osteogenic regulatory genes were enhanced by the surface morphology of the dental materials used.

Key words: Titanium, hydroxyapatite coating, gene expression profiling, cDNA microarray, anodization

Metal debris from total joint arthroplasty generated through wear and corrosion mechanisms can induce untoward effects in the peri-implant space. Particle

induced nonspecific inflammation is purportedly the dominant mechanism compromising the integrity of the bone-implant interface and can lead to peri-implant bone loss. The degree to which other concurrent processes, such as metal toxicity, negatively impact implant performance is unknown^{1,2}.

Titanium (Ti) and its alloys have been widely used for orthopedic implants that interact with bone cells *in vitro* and *in vivo*³. For decades, oral, maxillofacial, and orthopedic surgeons have placed dental implants, screws and plates, and prostheses to substitute lost teeth, to fix bone fragments, and to replace joints, respectively. Also, many surgical instruments, such as drills and saws, are made with Ti alloys. However, the exact effect of Ti on osteoblasts is still unknown⁴⁻⁶. Successful application of such materials for bone regeneration often involved mixing with autogenous bone, a source of osteoblastic cells and precursors⁴.

A positive voltage is applied to a Ti electrode placed in an electrolyte, an anodizing (anodic oxidation) process occurs, and a porous TiO₂ layer is produced on the Ti surface. The TiO₂ layer was found to significantly improve the cellular activities of Ti *in vitro* and the bone-implant bonding properties *in vivo*. These improvements were attributed to the increase in the surface roughness, as well as to the incorporation of calcium-phosphate coatings. The porous and rough morphology were increased the cell attachment and mechanical interlocking of the tissue and implant^{7,8}.

Surface topography may affect the formation of a fibrous capsule around implants, inflammatory response at tissue-implant interface, fibroblast attachment, angiogenesis, epithelial downgrowth around percutaneous devices, and many cellular processes such as cellular differentiation, DNA/RNA transcription, cell metabolism, protein production, and phenotypic expression^{3,5,9-11}. Diverse implant surface may contribute to the regulation of osteoblast differentiation by influencing the level of gene expression of key osteogenic factors^{11,12}. Morphometric analyses had shown differences in bone-implant contact percentages with the varying of surface characteristics, as well as a sensitivity of cells to surface topography^{13,14}. Gene expression in response to the placement of implants with different surface topographies¹⁵. Biomaterial composition and surface topography regulate cell attachment, focal contact formation and cytoskeletal organization with long-term effects on osteo-

blastic cell maturation, and subsequent mineralization¹⁶. The calcium-phosphate coatings, incorporated from the electrolyte into the coating layer, improved

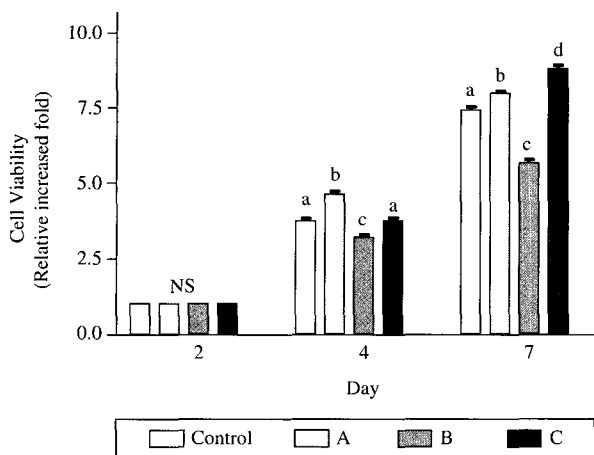


Fig. 1. Time and various Ti dependent effect on the cell viability of the MG63. The MG63 were treated with Control (non-HA coating on anodized surface), A (100 nm HA coating on anodized surface), B (500-700 nm HA coating on anodized surface), C (1 μ m HA coating on anodized surface). Different alphabetical letters indicate statistically one-way ANOVA, Duncan's multiple analysis significant differences ($P < 0.001$).

the osteoblast cell responses and further osseointegration. The existence of HA crystals on the anodized Ti was reported to improve the bone bonding of Ti implants *in vitro*^{7,8,17}.

We hypothesized that different size thin layer HA coatings on anodized Ti surface conditions would be associated with differential bone-matrix gene expression and interfacial strengths, which may lead to the development of more advanced therapeutic prosthetic interventions associated with dental implant therapy and tissue-engineering biological applications.

MG63 cells treated with B Ti grew slower than that incubated with A and C Ti. C surfaces displayed higher relative increased fold than other Ti surfaces during 7 days (Fig. 1). The viability appeared to be sensitive to the Ti surface used. Scanning electron microscopic (SEM) examinations revealed morphologic differences in the MG63 cells which adhered to various Ti surfaces. Cell growth was observed on control, A, B, and C. Fig. 2 presents the morphology and size of cell on the Ti surface. Control, A and C surfaces showed cell-matrix interaction. B surface showed cell-cell interaction. B sample was not observed pseudopodia. Control sample was observed that the shapes of cells having many pseudopodia are long and thin, and showed cell-matrix interaction and the smallest and round cell shape. C sample was showed cell-matrix

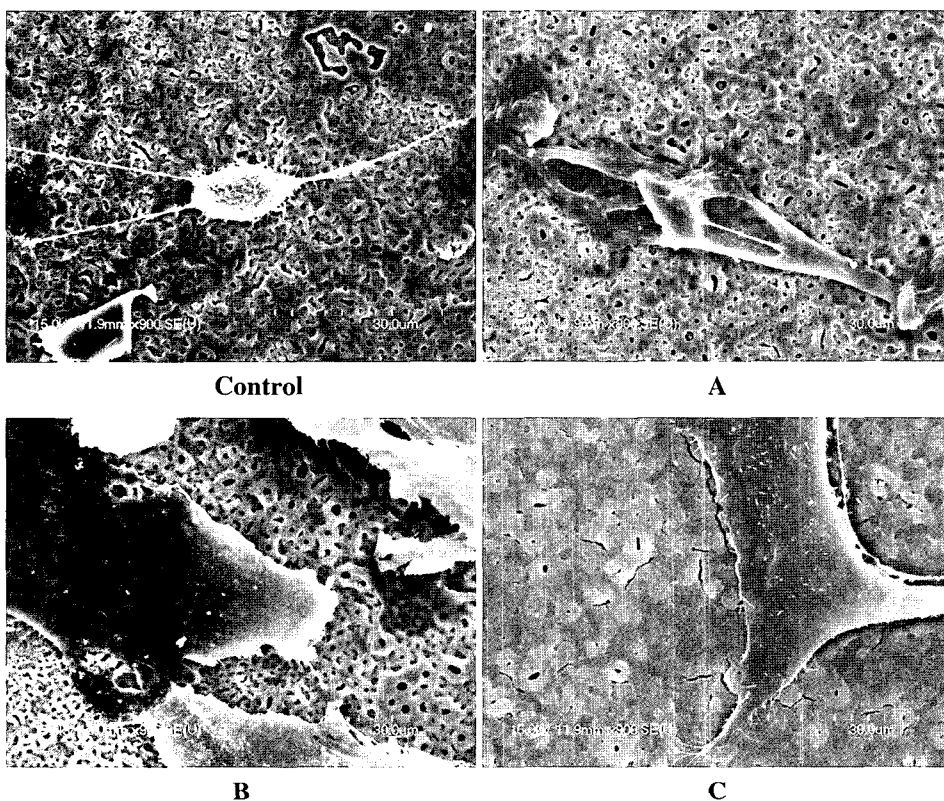


Fig. 2. SEM images of MG 63 cells attached on anodizing surfaces with different size HA coating (3day culture, $\times 900$): (a) the control (Non-HA coating on anodized surface) surface showing cell-matrix interaction; (b) the A (100 nm HA coating on anodized surface) surface showing cell-matrix interaction; the B (500-700 nm HA coating on anodized surface) surface showing cell-cell interaction; (c) the C (1 μ m HA coating on anodized surface) surface showing cell-matrix interaction.

interaction and the largest size of cell and the shortest pseudopodia. These results showed that the cells spread well on the B and C Ti surface, demonstrating good attachment potential to both control and C Ti.

Figure 3 is scatter plot for comparing the expression profiles of various thin layer HA coatings on anodized Ti and control. Regeneration analysis of Z scores from two independent samples of various thin layer

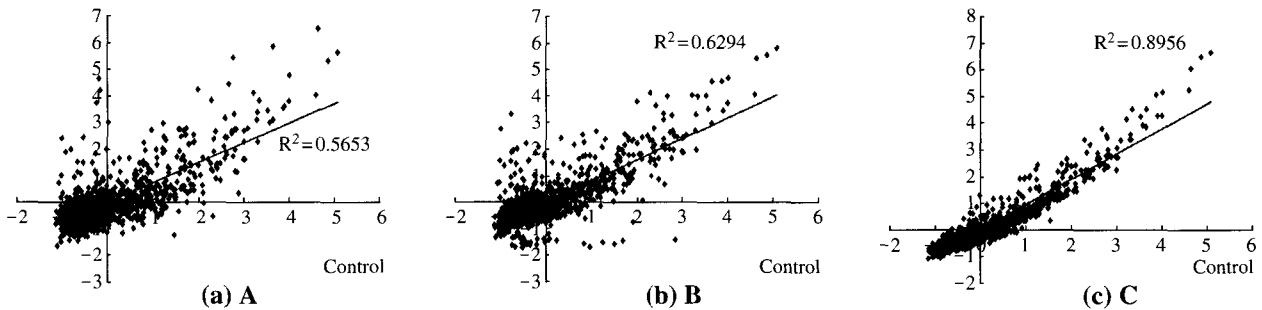


Fig. 3. Scatter plots for comparison of expression profile between control and different thin layer HA coating on anodized surface Ti. Expression profiles of non-HA coating (control) versus different thin layer HA coating on anodized surface Ti on MG63 cells. (a) A (100 nm HA coating on anodized surface) on MG63 cells versus control; (b) B (500-700 nm HA coating on anodized surface) on MG63 cells versus control; (c) C (1 μ m HA coating on anodized surface) on MG63 cells versus control are shown as bivariate scatterplots of 1,152 genes from the microarray. The values are corrected intensities relative to control, representing levels of expression for the DNA elements of the microarrays.

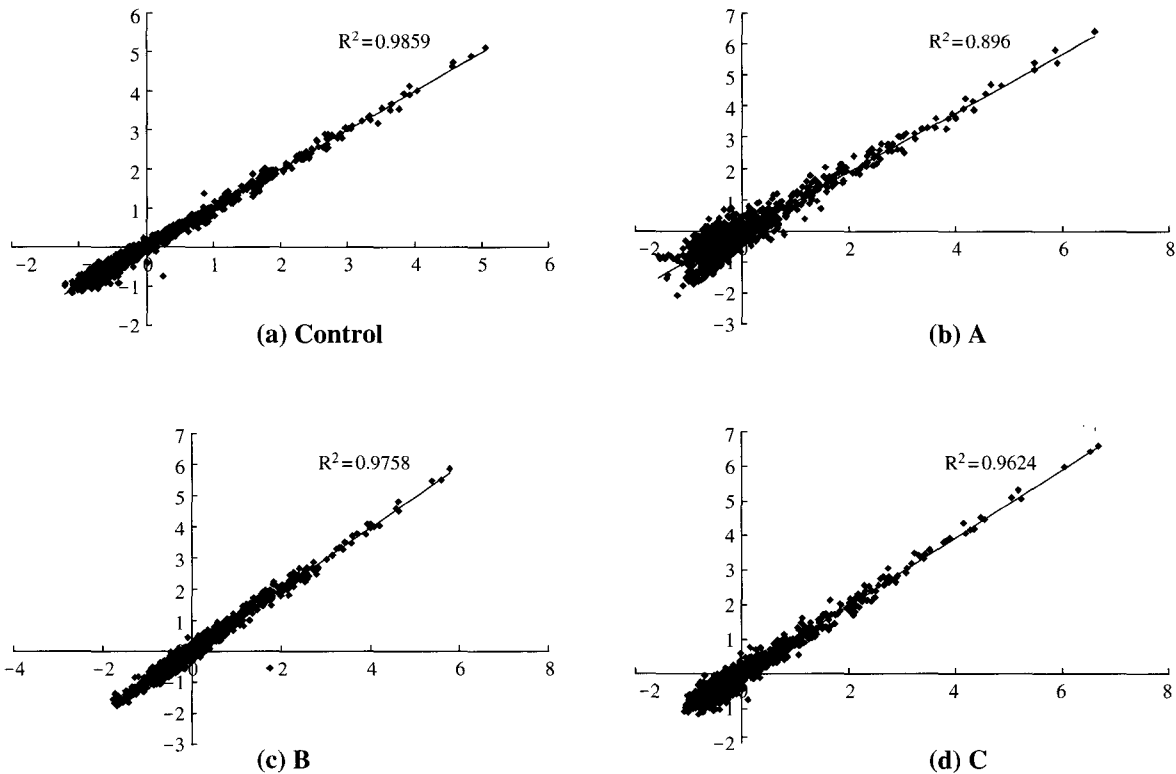
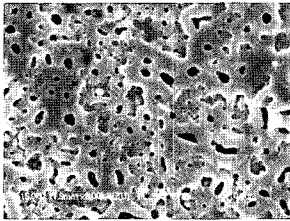
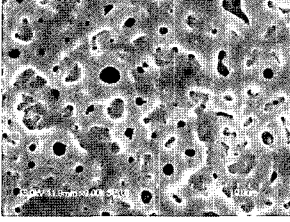
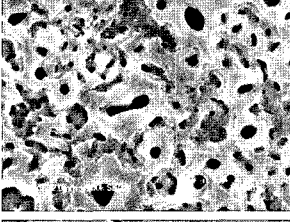
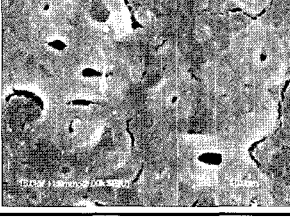


Fig. 4. Microarray reproducibility. Each microarray contains two identical grids. Regression analysis of Z scores from five samples of controls, A, B, and C coating on anodized surface Ti treated MG63 cells were performed. Z scores of individual genes from each member of duplicates were plotted, and the relationship between five samples was calculated to obtain R^2 . Based on R^2 , microarray hybridization patterns were found to be highly consistent between the samples. A perfect relationship between samples would be a slope of 1.

Table 1. The surface morphology & characteristics

	Coating	Surface morphology
Control	Non-HA coating on anodized surface	
A	100 nm HA coating on anodized surface	
B	500-700 nm HA coating on anodized surface	
C	1 μm HA coating on anodized surface	

*Magnification 2,000X, Ti surface morphology using a scanning electron microscopy (SEM).

HA coatings on anodized Ti and control were performed and Z scores of individual genes were plotted. To assess the reliability of microarray technique used, we calculated microarray reproducibility between duplicates (Fig. 4). The duplicate genetic elements for each microarray resulted in two separate Z normalizations and an average Z score for each gene. The scatter plot for Z scores in the cells grown on control, A, B, and C Ti samples showed R2 across duplicates of 0.99, 0.90, 0.98, and 0.96, respectively (Fig. 4). A perfect relationship between duplicates would be a slope of 1. The average coefficient of variation for duplicate Z scores within each microarray was below 10% approximately, indicating a high reliability of our microarray data. Table 2 shows the expression of various genes in different Ti surfaces compared with the control group.

Discussion

The frequently observed unwanted biological effects of different metals require *in vitro* and *in vivo* biological tests of any medical or dental device before its definite use in humans. Biological testing of medical and dental devices is necessary in order to evaluate the biological behaviour of biomaterials. The cell viability test using the MTT assay as assessed cell survival. *In vitro* cell viability test shown that control, A, B, and C have no cytotoxic effect (Fig. 1). And cell-matrix interaction morphology could be observed on the control and C surfaces, the surface morphology of which were observed by SEM to be rougher than those of other Ti samples (Table 1, Fig. 2). Osteoblastic cells began to secrete several extracellular matrix (ECM) proteins. They will also attach on the implant surface and are necessary for adhesion due to their specific binding to cell surface receptors. The formation of cell attachment to the alloys seems to be slower than on pure Ti. A reasonable explanation for this observation is that the formation of cell-implant contacts may be hampered on rough surfaces^{1,18} while Carinci *et al.*¹⁹ and Lossdorfer *et al.*²⁰ demonstrated that surface roughness affects proliferation, differentiation, local factor production. And alkaline phosphatase, osteocalcin, and Transforming Growth Factor beta were increased on the rougher surfaces. We also attempted to determine the effects of different Implant surfaces on the phenotype and gene expression of MG63 cells. In the experimental cultures, several genes were up-regulated or down-regulated. These genes were categorized depending on their functions, as follows (Table 2).

The FGFR (fibroblast growth factor receptor) family members include FGFR3 and FGFR12. The extracellular portion of the protein interacts with FGF, setting in motion a cascade of downstream signals, ultimately influencing mitogenesis and differentiation. This particular family member binds acidic and basic FGF hormone and plays a role in bone development and maintenance. FGF was combined with BMP, FGF prevented the differentiating action of BMP. The FGF was loosely bound to the matrix. Also, FGF signaling inhibited expression of alkaline phosphatase (ALKP) and blocked mineralization in osteoblastic cells²¹. In our study FGFR3 and FGFR12 were up-regulated in cultures grown on A. Integrins are heterodimeric integral membrane glycoproteins composed of an alpha chain and a beta chain that mediate cell-cell and cell-matrix adhesion.

The protein encoded by this gene, when bound to

Table 2. Up-and down regulated Genes of thin layer HA coatings on anodized surface

Genes	Abb.	Regulation profile and Z-ratio		
		A	B	C
Defense and stress related group				
mitogen-activated protein kinase kinase 7; JNKK2	MAP2K7	2.4	-0.05	1
small inducible cytokine A5 (RANTES)	CCL5	2.92	3.99	0.42
CD8 antigen, alpha polypeptide (p32)	CD8A	-2.11	-1.05	-1.28
chemokine (C-X3-C) receptor 1	CX3CR1	-2.16	-0.79	-1.39
TIA1 cytotoxic granule-associated RNA-binding protein-like 1	TIAL1	-2.16	-1.27	-1.02
protein phosphatase 1, regulatory subunit 10	PPP1R10	-2.39	-2.51	-1.72
superoxide dismutase 1, soluble (amyotrophic lateral sclerosis 1 (adult))	SOD1	0.04	2.76	0.71
mitogen-activated protein kinase kinase kinase 2	MAP4K2	0.57	4.15	0.78
adenosine A2a receptor	ADORA2A	-1.9	-4.81	-1.49
heat shock 90 kD protein 1, alpha	HSPCA	0	0.41	2.27
heat shock 70 kD protein 1	HSPA1	0.57	0.85	2.4
N-acylaminoacyl-peptide hydrolase	APEH	1.29	-0.15	2.68
monokine induced by gamma interferon	CXCL9	-0.65	-0.37	-2
sterile 20 (oxidant stress response kinase)	STK25	-1.63	-1.43	-2.24
chemokine (C-C motif) receptor 6	CCR6	-0.45	-0.94	-2.34
Apoptosis and anti-apoptosis related group				
tumor necrosis factor receptor superfamily, member 1B	TNFRSF1B	2.07	1.43	-0.82
synuclein, alpha (non A4 component of amyloid precursor)	SNCA	3.21	2.85	-0.08
apoptosis-associated tyrosine kinase	AATK	3.81	0.76	2.37
amyloid beta (A4) precursor protein (protease nexin-II)	APP	6.95	-0.38	-0.89
tumor suppressing subtransferable candidate 3	PHLDA2	-2.12	-1.14	-0.69
phosphatase and tensin homolog (mutated in multiple advanced cancers 1)	PTEN	-2.47	-1.13	-1.87
Bcl-2-interacting killer (apoptosis-inducing)	BIK	-2.51	-0.76	-1.48
tumor necrosis factor (ligand) superfamily, member 14	TNFSF14	-0.3	2.21	0.9
nucleolar protein 3 (apoptosis repressor with CARD domain)	NOL3	-0.7	3.08	-0.05
caspase 1, apoptosis-related cysteine protease	CASP1	-1.39	1.92	2.33
ubiquitin-binding protein p62	SQSTM1	0.77	1.63	2.87
neuroendocrine-specific protein C like (foocen)	RTN4	2.22	2.86	3.29
Bruton agammaglobulinemia tyrosine kinase	BTK	0.65	1.05	4.9
tumor necrosis factor receptor superfamily, member 10b	TNFRSF10B	-1.1	-0.75	-2.12
v-akt murine thymoma viral oncogene homolog 1	AKT1	-0.7	-1.27	-2.24
Inflammatory and immune related group				
lymphocyte antigen 64 (mouse) homolog, radioprotective, 105 kD	CD180	-2.02	-1.8	-0.96
pentaxin-related gene, rapidly induced by IL-1 beta	PTX3	-2.27	-0.56	-0.02
GRO2 oncogene	CXCL2	-0.55	3.64	0.36
interleukin 9	IL9	0.55	1.02	2.02
macrophage migration inhibitory factor (glycosylation-inhibiting factor)	MIF	0.25	0.56	2.97
platelet factor 4	PF4	-0.55	-0.9	-2.05
major histocompatibility complex, class II, DR beta 1	HLA-DRB1	-1.13	-0.14	-2.23
Transport related group				
ubiquinol-cytochrome c reductase, Rieske iron-sulfur polypeptide-like 1	UQCRFSL1	-2.08	-0.44	-1.11
frataxin	FXN	-2.17	-0.91	-1.83
P glycoprotein 1/multiple drug resistance 1	ABCB1	-0.08	4.2	0.13
vimentin	VIM	1.32	0.95	2.71
cholinergic receptor, nicotinic, alpha polypeptide 1 (muscle)	CHRNA1	-1.12	-1.11	-2.09
pleckstrin homology, Sec7 and coiled/coil domains1 (cytohesin 1)	PSCD1	-1.63	-1.1	-2.12
Metabolism related group				
iron-responsive element binding protein 2	IREB2	2.57	0	-0.12
retinol-binding protein 3, interstitial	RBP3	2.88	0.46	-0.02
defensin, alpha 6, Paneth cell-specific	DEFA6	3.13	1.42	2.59
8-oxoguanine DNA glycosylase	OGG1	-2.07	-1.21	-1.92
proteasome (prosome, macropain) subunit, alpha type, 1	PSMA1	-3.64	-0.69	-0.42
butyrophilin-like protein	BTNL	0.91	2.71	0.76
phosphodiesterase 1/nucleotide pyrophosphatase 2 (autotaxin)	ENPP2	0.52	2.75	0.41
ubiquitin specific protease 8	USP8	-0.07	1.38	3.28

Table 2. To be continued

Genes	Abb.	Regulation profile and Z-ratio		
		A	B	C
deoxyribonuclease II, lysosomal	DNASE2	0.95	-0.11	3.54
sialyltransferase 1 (beta-galactoside alpha-2, 6-sialyltransferase)	ST6GAL1	-1.83	-2.26	-2.05
peptidoglycan recognition protein	PGLYRP	-1.32	-0.47	-2.14
Cell proliferation and cell cycle related group				
midkine (neurite growth-promoting factor 2)	MDK	2.05	1.06	0.19
Wee1 + (<i>S. pombe</i>) homolog	WEE1	3	0.29	-0.27
cyclin D2	CCND2	0.81	2.04	1.08
E2F transcription factor 3	E2F3	0.24	3.28	-1.9
menage a trois 1 (CAK assembly factor)	MNAT1	1.09	3.56	0.16
budding uninhibited by benzimidazoles 1 (yeast homolog), beta singed (<i>Drosophila</i>)-like (sea urchin fascin homolog like)	BUB1B FSCN1	0.56 -0.46	-2.35 1.06	0.14 3.65
Cell differentiation and bone development related group				
fibroblast growth factor receptor 3	FGFR3	4.26	0.74	1.07
MAD (mothers against decapentaplegic, <i>Drosophila</i>) homolog 5	SMAD5	5.69	0.46	1.8
fibroblast growth factor 12	FGF12	6.24	0.15	0.26
protein tyrosine phosphatase, receptor type, N	PTPRN	-0.26	3.05	-0.28
latent transforming growth factor beta binding protein 1	LTBP1	-1.94	-4.32	-0.85
ephrin-A5	EFNA5	-0.11	0.74	2.1
S100 calcium-binding protein A10	S100A10	0.7	1	3.57
Cell adhesion related group				
CD4	CD4	2.68	1.18	4.21
selectin E (endothelial adhesion molecule 1)	SELE	3.14	0.41	-0.18
claudin 3	CLDN3	3.99	0.43	0.35
integrin, alpha 9	ITGA9	-2.34	-1.3	-1.41
gap junction protein, beta 2, 26 kD (connexin 26)	GJB2	1.09	6.39	0.59
integrin, alpha V (vitronectin receptor, alpha polypeptide, antigen CD51)	ITGAV	-1.23	-4.16	-1.31
integrin, alpha L	ITGAL	0.49	0.7	2.31
catenin (cadherin-associated protein)	CTNN	-1.65	-1.55	-2.01
Translation				
eukaryotic translation initiation factor 4A, isoform 1	EIF4A1	-2.46	-6.65	-0.22
ribosomal protein L5	RPL5	0.02	2.23	0.47
IMP (inosine monophosphate) dehydrogenase 1	IMPDH1	-0.2	2.85	0.28
ribosomal protein S6	RPS6	1.23	0.59	2.7
ribosomal protein L7a; SURF3	RPL7A	2.52	1.22	2.94
ribosomal protein S29	RPS29	-1.92	-1.47	-2.76
Transcription group				
retinoblastoma-like 1 (p107)	RBL1	2.53	-0.33	-2.18
MAD (mothers against decapentaplegic, <i>Drosophila</i>) homolog 9	SMAD9	2.56	2.08	3.47
CCAAT/enhancer binding protein (C/EBP), delta	CEBPD	2.91	-1.57	0.14
MAX protein; helix-loop-helix zipper protein (max)	MAX	4.87	5.86	0.37
v-rel avian reticuloendotheliosis viral oncogene homolog B	RELB	-2.28	-0.89	-0.82
v-rel avian reticuloendotheliosis viral oncogene homolog A	RELA	-2.32	-1.02	-1.85
zinc finger protein 49	ZNF49	-2.74	-0.28	-1.18
jun activation domain binding protein	JUN	-4.07	-0.41	0.18
heat shock transcription factor 4	HSF4	-1.17	-4.14	-0.54
POU domain, class 6, transcription factor 1	POU6F1	-1.72	-4.9	-1.81
nuclear transcription factor Y, beta	NFYB	1.25	0.87	2.39
transcription factor AP-2 alpha	TFAP2A	0.91	0.52	4
general transcription factor IIIA	GTF3A	-0.82	-1.01	-2.09
core-binding factor, runt domain, alpha subunit 2	RUNX1T1	-1.1	-1.83	-3.72
Signal transduction group				
G protein-coupled receptor 9	CXCR3	2.57	2.79	0.6
G protein-coupled receptor 37 (endothelin receptor type B-like)	GPR37	2.61	-0.2	-0.44
growth hormone releasing hormone	GHRH	-2.33	-1.64	-1.43
adrenergic, beta-2-, receptor, surface	ADRB2	-3.86	-1.22	-1.05

Table 2. To be continued

Genes	Abb.	Regulation profile and Z-ratio		
		A	B	C
platelet-activating factor receptor	PTAFR	1.96	2.14	2.51
tailless homolog (Drosophila)	NR2E1	1.62	2.21	1.7
interleukin 9 receptor	IL9R	0.83	2.42	1.65
interleukin 10	IL10	0.84	2.45	2.8
adaptor protein with pleckstrin homology and src homology 2 domains	APS	0.69	2.7	0.67
estrogen receptor 2 (ER beta)	ESR2	-0.27	2.71	0.45
protein kinase, cAMP-dependent, catalytic, beta	PRKACB	0.5	3.33	0.48
muscarinic acetylcholine receptor M1 (human)	CHRM1	0.85	3.49	-1.18
protein phosphatase 2, regulatory subunit B (B56), alpha isoform	PPP2R5A	0.18	4.13	0.25
regulator of G-protein signalling 1	RGS1	0.78	4.15	0.01
RAN, member RAS oncogene family	RAN	-0.65	-2.08	-0.93
interleukin 10 receptor, beta	IL10RB	-1.64	-2.08	-0.27
interleukin 2 receptor, alpha	IL2RA	-1.48	-2.1	0.17
mitogen-activated protein kinase kinase kinase 8	MAP3K8	-1.09	-2.33	-1.79
AXL receptor tyrosine kinase	AXL	-0.62	-2.64	-1.4
CD59 antigen p18-20	CD59	-0.58	-3.76	-1.29
src kinase-associated phosphoprotein of 55 kDa	SCAP1	1.08	1.07	3.48
thyroid stimulating hormone receptor	TSHR	0.81	1.12	4.77
prostaglandin E receptor 2 (subtype EP2), 53 kD	PTGER2	-2.01	-1.62	-2.44
DNA repair group				
damage-specific DNA binding protein 1 (127 kD)	DDB1	1.29	-2.31	0.2
high-mobility group (nonhistone chromosomal) protein 2	HMGB2	-0.14	0.64	2.04

the beta 1 chain, forms an integrin that is a receptor for VCAM1, cytotactin and osteopontin. Also, in our experiment, we noted the up-regulation of Integrin alpha L on C surfaces, a down-regulation of Integrin alpha 9 on A surfaces and a down-regulation of Integrin alpha V on B surfaces. Gap junctions were specialized structures on plasma membranes of contacting adherent cells. These structures were shown to consist of cell-to-cell channels. Proteins, called connexins, are designated by their molecular mass. Another system of nomenclature divides gap junction proteins into 2 categories, alpha and beta. Gap junction protein beta 2 is up-regulated in cultures grown on B.

Normal bone function is assured when there is equilibrium between bone formation and bone resorption. Apoptosis, or programmed cell death, is characterized by the activation of cysteine proteases called caspases, which cleave proteins essential for the survival of the cell. A member of this family, caspase-1, has been identified by its ability to proteolytically cleave and activate the inactive precursor of interleukin-1, a cytokine involved in the processes such as inflammation, septic shock, and wound healing. This gene has been shown to induce cell apoptosis and may function in various developmental stages¹⁴. We founded the C Ti induced apoptosis in osteoblasts in our *in vitro* model system, and caspase-1 was involved in this process. The increased susceptibility to apoptosis of the less

mature osteoblast could have important consequences for bone remodeling.

In our experiment, we observed several genes related with signal transduction for bone formation. However the expression of these genes such as MAP3K8, G protein coupled receptor 37, and G protein coupled receptor 9 were different according to different thin layer HA coatings on anodized surfaces.

MAP3K8 is a member of the kinase family. MAP kinases act as an integration point for multiple biochemical signals and are involved in a wide variety of cellular processes such as proliferation, differentiation, transcription regulation and development. MAP3K8 was identified by its oncogenic transforming activity in cells. The encoded protein is a member of the serine/threonine protein kinase family. This kinase can activate both the MAP kinase and JNK kinase pathways. This kinase was shown to activate I κ B kinases, and thus induce the nuclear production of NF- κ B. This kinase was also found to promote the production of TNF- α and IL-2 during T lymphocyte activation. Studies of a similar gene in rat suggested the direct involvement of this kinase in the proteolysis of NF- κ B1, p105 (NFKB1). This gene may also utilize a downstream in-frame translation start codon, and thus produce an isoform containing a shorter N-terminus. The shorter isoform has been shown to display weaker transforming activity^{16,21,22}. In our experiment, we noted

the down-regulation of MAP3K8 on B surfaces. CD183 is a G protein-coupled receptor with selectivity for three chemokines, termed IP10, Mig and I-TAC. IP10, Mig and I-TAC belong to the structural subfamily of CXC chemokines, in which a single amino acid residue separates the first two of four highly conserved Cys residues. Historically, CD183 is the third CXC chemokine receptor discovered and, therefore, commonly designated as CXCR3. Binding of chemokines to CD183 induces cellular responses that are involved in leukocyte traffic, most notably integrin activation, cytoskeletal changes and chemotactic migration. Inhibition by Bordetella pertussis toxin suggests that heterotrimeric G protein of the Gi-subclass couple to CD183. Signal transduction has not been further analyzed but may include the same enzymes that were identified in the signaling cascade induced by other chemokine receptors. As a consequence of chemokine-induced cellular desensitization (phosphorylation-dependent receptor internalization), cellular responses are typically rapid and short in duration. Cellular responsiveness is restored after dephosphorylation of intracellular receptors and subsequent recycling to the cell surface. A hallmark of CD183 is its prominent expression in *in vitro* cultured effector/memory T cells, and in T cells present in many types of inflamed tissues. In addition, IP10, Mig and I-TAC are commonly produced by local cells in inflammatory lesion, suggesting that CD183 and its chemokines participate in the recruitment of inflammatory cells¹⁶. In our experiment, we noted the up-regulation of G protein coupled receptor 37 on surfaces, and an up-regulation of G protein coupled receptor 9 on A and B surfaces.

We demonstrated that various thin layer HA coatings on anodized surfaces were capable of modulating the expressions of some genes. Our results indicated that the gene encoding bone formation-related proteins was up-regulated mainly in the A and C cultures. Carinci *et al.*¹⁹ reported that surface topography exerted influences on the frequency and amount of formed bone, and that mineralized products can be guided by the surface topography of the implant. It has also been determined that bone formation induced by osteoblast-like cells at the implant-cell interface is quite a complex process, and involves a host of cellular functions, including cellular attachment, migration, and proliferation, followed by the expression of markers for osteoblast phenotype, and the synthesis, deposition, and mineralization of the bone matrix²³. We believe that the data reported that the function of the signaling pathway in osteoblast differentiation may contribute to the identification of new therapeutics, for the treatment of poor bone qual-

ity. This study may provide dentists with a great deal of useful information for the improvement of present biomaterials, as well as the future development of new biomaterials.

Methods

Titanium Preparation

All Ti substrates were constructed from grade 4 commercially pure titanium (cp Ti). The materials were Ti discs with a diameter of 8 mm, a thickness of 1.5 mm, in a coin-shaped circle. The Ti samples used in the experiments had different surfaces (control; non HA coating on anodized surface, A; 100 nm HA coating on anodized surface, B; 500-700 nm HA coating on anodized surface, C; 1 μ m HA coating on anodized surface,). Table 1 shows these surface properties. After surface preparation, these samples were washed with distilled water, and then rinsed thoroughly in 70% ethanol and absolute ethanol. Prior to cell culturing, the discs were sterilized by γ -rays.

Cell Culture

MG63 cell line was obtained from the American Type Culture Collection (Rockville, MD). MG63 cells were cultured on dental materials with different surfaces (control, A, B, and C). The MG63 cells (KCLB[®] Korean Cell Line Bank) were cultured in (Dulbecco Eagle's minimum essential medium, Biowhittaker, Belgium) MEM medium with 10% fetal bovine serum, and antibiotics (Penicillin 100 U/mL and Streptomycin 100 μ g/mL, Invitrogen, Milano, Italy) were seeded at 1×10^4 /mL in a humidified atmosphere of 5% CO₂ at 37°C. These materials were placed in a 24-multiwell plate (NUNC[™], Denmark). 1 μ L of cell suspension was applied carefully to a 24-multiwell and the cells had been allowed to attach for 3 days to the MG63.

Cell Viability

The MTT assay was carried out as described previously^{24,25} with some modifications. All Ti substrates were placed in a 24-multiwell plate (Corning, USA). MG63 cells were seeded in seven 24-well plates, and each well contained 1.2×10^3 cells. At the time of analysis, MTT assays were essentially performed according to Mosmann (1983). Triplicate wells were used for each experimental condition. Absorbance was measured in a Microplate Reader (Molecular Devices, Spectra max 384 plus, Union City, CA, USA) at a wavelength of 540 nm.

Scanning Electron Microscopy(SEM)

SEM (S-4700, HITACHI, Tokyo, Japan) was employed in order to determine the morphological characteristics of cells in culture. The advantages associated with SEM include its large depth of focus, high lateral resolution down to the nanometer range, the feasibility to study structures with high aspect ratios, and the direct production of surface images.

Human cDNA Microarray

A MG63 cDNA microarray was derived principally from a commercially available master set of approximately 15,000 human verified-sequences (Research Genetics, Inc., Huntsville, AL). The 15,000 human cDNA clone set was sorted for a list of genes (1,152 elements) representing families such as differentiation, development, proliferation, transformation, cell cycle progression, immune response, transcription and translation factors, oncogenes, and molecules involved in cell growth and maintenance. PCR-amplified cDNAs were spotted on nylon membranes. The general methodology of arraying is based on the procedures of DeRisi *et al.*²⁶.

RNA Preparation and cDNA Radiolabeling

The RNA was isolated from cultured cells which adhered to the retrieved implants of different surfaces (control, A, B, and C) with Trizol (Invitrogen, Milano, Italy). RNA was quantified via UV spectrophotometry (spectrophotometer-DU650; Beckman, Somerset, NJ, USA). After quantification, 3-10 µg of total RNAs prepared from the MG63-treated dental materials with different surfaces (control, A, B, and C) were used for each sample for adjustment of different cell numbers. To synthesize ³³P-labeled cDNAs, quantified RNA were labeled in a reverse transcription reaction containing 5X first strand PCR buffer, 1 µg of 24-mer poly dT primer, 4 µL of 20 mM each dNTP excluding dCTP, 4 µL of 0.1 M DTT, 40 U of RNase inhibitor, 6 µL of 3000 Ci/mmol α-³³P dCTP to a final volume of 40 µL. The mixture was heated at 65°C for 5 min, followed by incubation at 42°C for 3 min. Two µL (specific activity: 200,000 U/mL) of Superscript II reverse transcriptase (Invitrogen, Milano, Italy) was then added and the samples were incubated for 30 min at 42°C, followed by the addition of 2 µL of Superscript II reverse transcriptase and another 30 min of incubation. Five µL of 0.5 M EDTA was added to chelate divalent cations. After the addition of 10 µL of 0.1 M NaOH, the samples were incubated at 65°C for 30 min to hydrolyze remaining RNA. Following the addition of 25 µL of 1 M Tris (pH 8.0), the samples were purified using Bio-Rad 6 purification columns (Hercules, CA, USA). This resulted in 5 × 10⁶

to 3 × 10⁷ cpm per reaction²⁷.

Hybridization and Scanning

cDNA microarrays were pre-hybridized in hybridization buffer containing 4.0 mL Microhyb (Invitrogen, Milano, Italy), 10 µL of 10 mg/mL human Cot 1 DNA (Invitrogen, Milano, Italy), and 10 µL of 8 mg/mL poly dA (Pharmacia, Peapack, NJ). Both Cot 1 and poly dA were denatured at 95°C for 5 min prior to use. After 4 h of pre-hybridization at 42°C, approximately 10⁷ cpm/mL of heat-denatured (95°C, 5 min) probes were added and incubation continued for 17 h at 42°C. Hybridized arrays were washed three times in 2X SSC and 0.1% SDS for 15 min at room temperature. The microarrays were exposed to phosphorimager screens for 1-5 days, and the screens were then scanned in a FLA-8000 (Fuji Photo Film Co., Japan) at 50 µm resolution^{27,28}.

Data Analysis

Microarray images were trimmed and rotated for further analysis using L-Processor system (Fuji Photo Film Co., Japan). Gene expression of each microarray was captured by the intensity of each spot produced by radioactive isotopes. Pixels per spot were counted by Arraygauge (Fuji Photo Film Co., Japan) and exported to Microsoft Excel (Microsoft, Seattle, WA, USA). The data were normalized with Z transformation to obtain Z scores by subtracting each average of gene intensity and dividing with each standard deviation. Z scores provide each of 2,304 spots (two sets of 1,152 genes) genes with the distance from the average intensity and were expressed in units of standard deviation. Thus, each Z score provides flexibility to compare different sets of microarray experiments, by adjusting differences in hybridization intensities. Gene expression difference as compared with untreated control cells were calculated by comprising Z score differences (Z differences) among the same genes. This facilitates comparing each gene that had been up- or downregulated as compared with the control cells. Z differences were calculated first by subtracting Z scores of the controls from each Z score of the sample. These differences were normalized again to distribute their position by subtracting the average Z difference and dividing with the standard deviation of the Z differences. These distributions represent the Z ratio value and provide the efficiency for comparing each microarray experiment²⁷. Scatter plots of intensity values were produced by Spotfire (Spotfire, Inc., Cambridge, MA)²⁹. Cluster analysis was performed on the Z-transformed microarray data by using two programs available as shareware from Michael Eisen's laboratory (<http://rana.lbl.gov>). Clu-

stering of changes in gene expression was determined by using a public domain cluster based on pair wise complete-linkage cluster analysis³⁰.

Statistical Analysis

For any given experiment, each data point represents the mean \pm SEM (standard error of the mean) from seven individual cultures. After a significant ANOVA (analysis of variance), Duncan's multiple range tests were performed in order to determine the significance of the differences in the cell number means among a variety of Ti surfaces. Standard software (SPSS, Ver 11.0) was used for the statistical analysis in this study and differences were considered significant at the 5% level. P values of <0.05 were considered to be statistically significant.

Acknowledgements

We thank Dr. Yoon S. Cho-Chung (Cellular Biochemistry Section, Basic Research Laboratory, CCR, NCI, NIH, Bethesda, MD) and Dr. Kevin G. Becker (DNA Array Unit, NIA, NIH, Baltimore, MD) for valuable advices on cDNA microarray. This study was supported by a grant of Medical Research Center for Environmental Toxicogenomic and Proteomics, funded by Korea Science and Engineering Foundations and Ministry of Science & Technology, a grant of the Korea Health 21 R&D Project, Ministry of Health & Welfare, Republic of Korea (Hmp-00-GN-01-0002 & KPGRN-R-04), a Korea Institute of Science & Technology Evaluation and Planning (KISTEP) and Ministry of Science & Technology (MOST), Korean government, through its National Nuclear Technology Program, and a grant No. R01-2001-000-00212-0 from the Basic Research Program of the Korea Science & Engineering Foundation.

References

- Hornez, J.C., *et al.*, Multiple parameter cytotoxicity index on dental alloys and pure metals. *Biomol. Eng.* **19**(2-6), 103-117 (2002).
- Hallab, N.J. *et al.* Effects of soluble metals on human peri-implant cells. *J. Biomed. Mater. Res. A.* **74**(1), 124-140 (2005).
- Shah, A.K., *et al.* High-resolution morphometric analysis of human osteoblastic cell adhesion on clinically relevant orthopedic alloys. *Bone.* **24**(5) 499-506 (1999).
- Cooper, L.F. *et al.* Incipient analysis of mesenchymal stem-cell-derived osteogenesis. *J. Dent. Res.* **80**(1), 314-320 (2001).
- Carinci, F. *et al.* Titanium-cell interaction: analysis of gene expression profiling. *J. Biomed. Mater. Res.* **66B**(1), 341-346 (2003).
- Viornerly, C. *et al.* Osteoblast culture on polished titanium disks modified with phosphonic acids. *J. Biomed. Mater. Res.* **62**(1), 149-155 (2002).
- Son, W.W. *et al.* *In vivo* histological response to anodized and anodized/hydrothermally treated titanium implants. *J. Biomed. Mater. Res. B Appl. Biomater.* **66**(2), 520-525 (2003).
- Li, L.H. *et al.* Biocompatibility of titanium implants modified by microarc oxidation and hydroxyapatite coating. *J. Biomed. Mater. Res. A.* **73**(1), 48-54 (2005).
- Kim, H.K., Jang, J.W. & Lee, C.H. Surface modification of implant materials and its effect on attachment and proliferation of bone cells. *J. Mater. Sci. Mater. Med.* **15**(7), 825-830 (2004).
- Ogawa, T., Sukotjo, C. & Nishimura, I. Modulated bone matrix-related gene expression is associated with differences in interfacial strength of different implant surface roughness. *J. Prosthodont.* **11**(4), 241-247 (2002).
- Schneider, G.B. *et al.* Implant surface roughness affects osteoblast gene expression. *J. Dent. Res.* **82**(5), 372-376 (2003).
- Carinci, F. *et al.* Zirconium oxide: analysis of MG63 osteoblast-like cell response by means of a microarray technology. *Biomaterials.* **25**(2), 215-228 (2004).
- Orsini, G. *et al.* Surface analysis of machined versus sandblasted and acid-etched titanium implants. *Int. J. Oral Maxillofac Implants.* **15**(6), 779-784 (2000).
- Son, W.W. *et al.* *In vivo* histological response to anodized and anodized/hydrothermally treated titanium implants. *J. Biomed. Mater. Res. B Appl. Biomater.* **66**(2), 520-525 (2003).
- Ogawa, T. & Nishimura, I. Different bone integration profiles of turned and acid-etched implants associated with modulated expression of extracellular matrix genes. *Int J Oral Maxillofac Implant.* **18**(2), 200-210 (2003).
- Carinci, F. *et al.* Analysis of osteoblast-like MG63 cells' response to a rough implant surface by means of DNA microarray. *J. Oral Implantol.* **29**(5), 215-220 (2003).
- Gopal, J. *et al.* Photocatalytic inhibition of microbial adhesion by anodized titanium. *Biofouling.* **20**(3), 167-175 (2004).
- Monsees, T.K. *et al.* Effects of different titanium alloys and nanosize surface patterning on adhesion, differentiation, and orientation of osteoblast-like cells. *Cells Tissues Organs.* **180**(2), 81-95 (2005).
- Carinci, F., *et al.*, Analysis of MG63 osteoblastic-cell response to a new nanoporous implant surface by means of a microarray technology. *Clin. Oral Implants Res.* **15**(2), 180-186 (2004).
- Lossdorfer, S. *et al.* Microrough implant surface topographies increase osteogenesis by reducing osteoclast formation and activity. *J. Biomed. Mater. Res.* **70A**(3), 361-369 (2004).

21. Chaudhary, L.R., Hofmeister, A.M. & Hruska, K.A. Differential growth factor control of bone formation through osteoprogenitor differentiation. *Bone*. **34**(3), 402-411 (2004).
22. Kim *et al.* Effect of various implant coatings on biological responses in MG63 using cDNA microarray. *J. Oral Rehabil.* In press (2005).
23. Mustafa, K. *et al.* Determining optimal surface roughness of TiO₂ blasted titanium implant material for attachment, proliferation and differentiation of cells derived from human mandibular alveolar bone. *Clin. Oral Implants Res.* **12**(5), 515-525 (2001).
24. Mosmann, T. Rapid colorimetric assay for cellular growth and survival: application to proliferation and cytotoxicity assays. *J. Immunol. Methods*. **65**(1-2), 55-63 (1983).
25. Taira, M. *et al.* Effects of two vitamins, two growth factors and dexamethasone on the proliferation of rat bone marrow stromal cells and osteoblastic MC3T3-E1 cells. *J. Oral Rehabil.* **30**(7), 697-701 (2003).
26. DeRisi, J. *et al.* Use of a cDNA microarray to analyse gene expression patterns in human cancer. *Nat. Genet.* **14**(4), 457-460 (1996).
27. Vawter, M.P. *et al.* Application of cDNA microarrays to examine gene expression differences in schizophrenia. *Brain Res. Bull.* **55**(5), 641-650 (2001).
28. Park, G.H. *et al.* Genome-wide expression profiling of 8-chloroadenosine- and 8-chloro-cAMP-treated human neuroblastoma cells using radioactive human cDNA microarray. *Exp. Mol. Med.* **34**(3), 184-193 (2002).
29. Tanaka, T.S. *et al.* Genome-wide expression profiling of mid-gestation placenta and embryo using a 15,000 mouse developmental cDNA microarray. *Proc. Natl. Acad. Sci. U S A.* **97**(16), 9127-9132 (2000).
30. Eisen, M.B. *et al.* Cluster analysis and display of genome-wide expression patterns. *Proc. Natl. Acad. Sci. U S A.* **95**(25), 14863-14868 (1998).